

---

# Starspots, chromospheric emission lines, and flares of zero-age main-sequence stars

Mai Yamashita<sup>1</sup>, Yoichi Itoh<sup>1</sup>, Yumiko Oasa<sup>2</sup>

<sup>1</sup>Nishi-Harima Astronomical Observatory, Center for Astronomy, University of Hyogo, 407-2 Nishigaichi, Sayo, Sayo, Hyogo 679-5313

<sup>2</sup>Faculty of Education, Saitama University, 255 Shimo-Okubo, Sakura, Saitama, Saitama, Japan

\*E-mail: yamashita@nhao.jp

Received (2022 May 26); Accepted (2022 Aug 09)

## Abstract

Zero-age main-sequence (ZAMS) stars are considered to have enormous starspots and show strong chromospheric emission lines because of their strong surface magnetic field. We discuss the dynamo activities of ZAMS stars with respect to their periodic light variation caused by a starspot and with respect to the strength of the chromospheric emission lines. The light curves of 33 ZAMS stars in IC 2391 and IC 2602 were obtained from *TESS* photometric data. The light curves can be grouped into the following four categories: single frequency, possible shape changer, beater, and complex variability. The amplitudes of the light curves are 0.001 – 0.145 mag, similar to those of ZAMS stars in Pleiades. The starspot coverages are 0.1 – 21%. We found that the light variations and Ca II emission line strength of ZAMS stars in IC 2391, IC 2602, and the Pleiades cluster are as large as those of the most active superflare stars and two orders larger than those of the Sun, and are located on the extensions of the superflare stars. These results suggest that superflare stars link the properties of the Sun to those of the ZAMS stars of ages between 30 and 120 Myr. ZAMS stars with a single frequency or possible shape change in the light curve tend to have both large light variation, indicating large spot coverage, and saturated Ca II emission line strength. ZAMS stars with beat or complex variability have small spot coverage and a faint Ca II emission line. We also detected 21 flares in the *TESS* light curves of 12 ZAMS stars in IC 2391 and IC 2602, where most of

these stars have saturated chromospheric Ca II emission lines. The energies of the flares are estimated to be  $\sim 10^{33} - 10^{35}$  erg, which is comparable with the energy of a superflare.

**Key words:** stars: chromospheres — stars: activity — techniques: photometric

---

## 1 Introduction

The chromosphere is the active atmosphere in which atoms emit some permitted lines, such as H $\alpha$  and Ca II. It is claimed that chromospheric activity is driven by the magnetic fields induced by the dynamo process. In the dynamo process, the Coriolis force (= rotational moment  $\times$  convection velocity) balances the Lorentz force (= current  $\times$  magnetic strength / density of plasma) (Baliunas et al. 1996). Stellar rotation and convection are considered to be the main processes that drive the evolution of magnetic activities. Noyes et al. (1984) used the Rossby number,  $N_R$ , as an indicator of magnetic activity. It is defined as  $P/\tau_c$ , where  $P$  is the stellar rotational period and  $\tau_c$  is the convective turnover time.  $N_R$  can be approximated as the inverse square of the dynamo number,  $N_D$ , the wave solution of the dynamo equation. Magnetic fields develop when  $|N_D| > 1$ .

Chromospheric emission lines are observational evidence of a strong magnetic field. The relationship between chromospheric line strength and the Rossby number has been examined for zero-age main-sequence (ZAMS) stars. Marsden et al. (2009) detected Ca II infrared triplet (IRT;  $\lambda 8498, 8542, 8662$  Å) emission lines from low-mass stars in the young open clusters IC 2391 and IC 2602. The cluster members are considered to be on ZAMS or in the last evolution phase prior to ZAMS. They calculated  $R'_{\text{IRT}}$  from the equivalent widths (EQWs).  $R'_{\text{IRT}}$  describes the ratio of the surface flux of the Ca II IRT emission lines to the stellar bolometric luminosity. They found that  $R'_{\text{IRT}}$  decreases with increasing  $N_R$  for stars with  $N_R \geq 10^{-1.1}$ . This region is called the unsaturated regime. In contrast,  $R'_{\text{IRT}}$  is constant at levels of approximately  $10^{-4.2}$  for stars with  $N_R \leq 10^{-1.1}$ . This region is called the saturated regime. Marsden et al. (2009) suggested that the chromosphere is completely filled by the emitting regions for the stars in the saturated regime. Recently, Fritzewski et al. (2021) found that some of the FGKM-type stars in the young open cluster NGC 3532 (300 Myr) also show saturation at  $R'_{\text{IRT}} \sim 10^{-3.7}$ . Yamashita et al. (2020) investigated the relationship between  $N_R$  and the Ca II IRT emission lines of 60 pre-main sequence (PMS) stars. Only three PMS stars showed broad and strong emissions, indicative of large mass accretion. Most of the PMS stars presented narrow and weak emissions, suggesting that their emission lines are formed in the chromosphere. All their Ca II IRT emission lines have  $R'_{\text{IRT}} \sim 10^{-4.2}$ , which is as large as the maximum  $R'_{\text{IRT}}$  of ZAMS stars. The

PMS stars show  $N_R < 10^{-0.8}$  and constant  $R'_{\text{IRT}}$  against  $N_R$ , i.e., their Ca II IRT emission lines are saturated. Yamashita et al. (2022) (hereafter Paper I) investigated the infrared Mg I emission lines at 8807 Å of 47 ZAMS stars in IC 2391 and IC 2602 using the archive data of the Anglo-Australian Telescope at the University College London Echelle Spectrograph. They found that ZAMS stars with smaller Rossby numbers show stronger Mg I emission lines, even for stars located in the Ca II saturated region.

Regarding the solar disk, it is known that spots are surrounded by emission regions, such as faculae in the photosphere and plages in the chromosphere. Other observational evidence for the strong magnetic field of a star includes the periodic light variation caused by a starspot. The amplitude of the solar brightness variation caused by sunspots on the rotating solar surface is 0.01 – 0.1% (Lanza et al. 2003). In recent years, *Kepler* and Transiting Exoplanet Survey Satellite (*TESS*, Ricker et al. 2015) satellites have been utilized to investigate stellar magnetic activities. The typical photometric precision of *Kepler* is 0.01% for a star of 12 mag (Koch et al. 2010). The time resolution of *Kepler* is approximately 30 minutes and 1 minutes. Rebull et al. (2016a) presented *K2* light curves for F-, G-, K-, and M-type ZAMS stars in the Pleiades cluster. The rotational periods ranged from 0.082 d to 22.14 d. The amplitude of the brightness ranged from 0.001 mag to 0.556 mag. Rebull et al. (2016a) and Stauffer et al. (2016) investigated the relationship between the rotational periods and shapes of the light curves for ZAMS stars in the Pleiades cluster and found that approximately half of the F-, G-, and K-type ZAMS stars rotating rapidly have sinusoidal light curves.

Flares are also observational evidence for a strong magnetic field. Maehara et al. (2012) detected 365 flares with *Kepler* data regarding 148 solar-type stars. The releasing energy of the flare is 100 times larger than those of solar flares. Such objects are called superflare stars. Notsu et al. (2015b) found that the Sun and superflare stars show a positive correlation between the amplitude of the light curve and the  $r_0(8542)$  index, the residual core flux of the Ca II IRT normalized by the continuum level at the line core. This correlation means that superflare stars have large starspots and high magnetic activity compared to the Sun. Ilin et al. (2021) detected 3844 flares from *K2* data from 2111 objects associated with open clusters. The cluster ages range from 0.1 Gyr to 3.6 Gyr. They found that flaring rates decline with age and decline faster for stars with higher mass.

We discuss the relationship between the periodic light variation caused by a starspot, the strength of the chromospheric emission lines, and flare events. We measured the light variations of 33 ZAMS stars in IC 2391 and IC 2602 with *TESS* photometric data. In the next section, we describe the photometric data reduction procedure. In Section 3, we present the results, and in Section 4, we discuss the dynamo activities in terms of the light variation, the Rossby number, the chromospheric emission strength, and the flares.

## 2 Data Sets and Data Reduction

### 2.1 Stellar parameters

Our targets are F-, K-, and G-type ZAMS stars in IC 2391 ( $50 \pm 5$  Myr; Barrado y Navascues et al. 2004) and IC 2602 ( $30 \pm 5$  Myr; Stauffer et al. 1997). The metallicity of both clusters has been determined to be similar to that of the Sun, which is  $[\text{Fe}/\text{H}] = -0.01 \pm 0.02$  for IC 2391 (D’Orazi & Randich 2009) and  $[\text{Fe}/\text{H}] = 0.00 \pm 0.01$  for IC 2602 (Randich et al. 2001). A total of 44 ZAMS stars have been confirmed as single stars in the IC 2391 and IC 2602 members based on the strength of the lithium  $6708 \text{ \AA}$  absorption line (Marsden et al. 2009). In Paper I, we examined the proper motion and radial velocity of those stars, and five ZAMS stars were removed from our target list. The 39 targets investigated in this study are presented in table 1.

### 2.2 Data Reduction

The members of IC 2391 and IC 2602 were observed in the long-cadence (1800-s exposure) mode of *TESS* Sectors 8 and 10, which extended from the 2nd to the 27th of February 2019, and from the 26th of March 2019 to the 21st of April 2019, respectively. These data were retrieved from the Multimission Archive at the Space Telescope Science Institute. We conducted principal component analysis using ELEANOR, an open-source tool for extracting light curves from *TESS* full-frame images (Feinstein et al. 2019). ELEANOR enables us to model a 2D background, and remove the extended point-spread function of bright stars across the *TESS* images. However *TESS* pixels are substantially larger than that of *Kepler*. We excluded 6 ZAMS stars from the targets because another star whose magnitude is brighter than  $< 3 + V$  mag of the ZAMS star is located in the aperture of the ZAMS star.

First, we search for periodic signals and obtain the amplitudes of the light curves. We calculated the standard deviation of the flux,  $\sigma_1$ , and removed the flux data points greater than  $3\sigma_1$  above the average. As described in Paper I, we searched for periodic signals by conducting Lomb–Scargle periodogram analysis (Scargle 1982). We note that VXR PSPC 44 showed beating signatures in its light curve; we adopted the period for the second maximum of the power as the period of the object. We calculated the amplitudes of the light curves by taking the 90th percentile flux and subtracting it from the 10th percentile flux.  $P$  was judged to be accurate if  $\text{amplitude}/\text{mean flux error} \geq 10$ . The periods derived by us show good correlation with the periods measured by Patten & Simon (1996) and Barnes et al. (1999), with a correlation coefficient of 0.997.

Next, we detected sudden brightenings as flares. Starting from the original light curves (including  $3\sigma_1$  outliers), first we removed the rotational light variations as described below (figure 1).

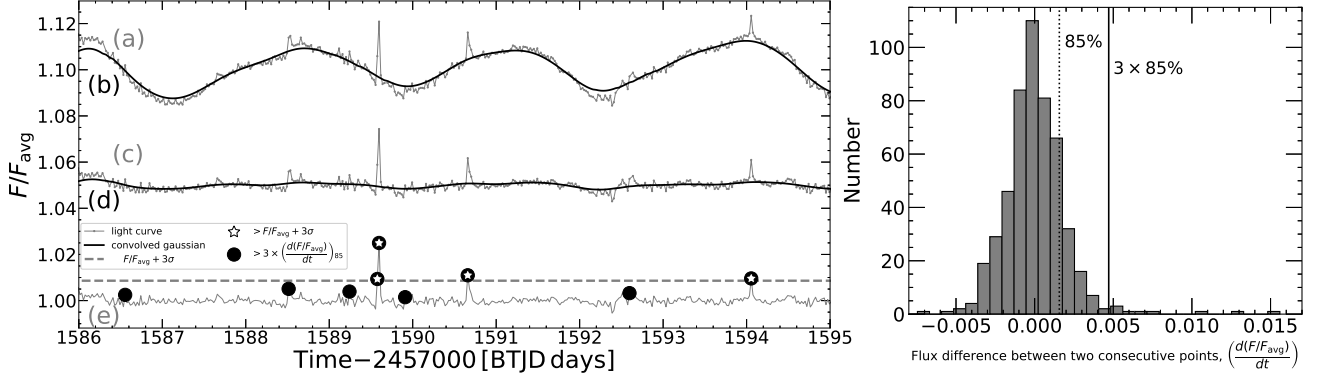


**Fig. 1:** Light curve of the ZAMS star, [RSP 95] 14. Horizontal and vertical axes correspond to days and normalized flux. Top) The original light curve is shown with the gray solid line (a). This is divided by the median of the counts and normalized to 1. The thick black line is the Gaussian convolved light curve (b). The standard deviation of the Gaussian function is set to 300 mins. These lines are shifted by +0.10 for display purposes. Middle) The ratio between the original light curve and the Gaussian convolved light curve shown in the top panel is presented with the gray solid line (c). The thick black line is the Gaussian convolved light curve of the gray solid line (d). The standard deviation of the Gaussian function is set to 300 mins. These lines are shifted by +0.05 for display purposes. Bottom) The ratio between the light curve shown in the middle and the second Gaussian convolved light curve is shown with the gray solid line (e). The dashed line denotes  $1 + 3\sigma$  of the gray line. The open symbols represent data points greater than the dashed line. The filled circles represent data points whose brightness change is greater than the threshold of the change of the brightness. The three sudden brightenings (four points) are detected as flares. The histogram in the right panel shows the number distribution of the flux differences between all pairs of two consecutive data points. The dotted line shows the top 15% of the distribution. The solid line shows the threshold of the change of the brightness, three times in the top 15% of the distribution.

*TESS* data was not obtained for several days in the middle of the observation period. We separated the light curve at the center time. Each light curve was divided by the median of the counts and normalized to 1 (figure 1 (a)). Each light curve was convolved with a Gaussian function (figure 1 (b)) and divided by the convolved light curve. The derived light curve (figure 1 (c)) was again convolved with a Gaussian function (figure 1 (d)). We set the standard deviation of the Gaussian function to between 15 mins and 2.5 days for each light curve. With these processes, no rotational light variation remained in the light curve, and most of the data points were set around unity (figure 1 (e)). We then measured the standard deviation of the counts in the light curve,  $\sigma_2$ , for each ZAMS star.

We defined two thresholds for flare detection. The first threshold is the height of sudden brightening. After removing the rotational light variations, we searched for sudden brightenings whose relative flux exceeded  $1 + 3\sigma_2$  for at least one data point. The second threshold is the change of the brightness. We calculated the brightness changes between all pairs of consecutive data points.

We searched for any brightness change that occurred more than three times in the top 15% of the distribution (the solid line in the right panel of figure 1). We identified a sudden brightening that exceeded both thresholds as a flare. The time at which the flux first exceeded the first threshold,  $1 + 3\sigma_2$  of the relative flux, was determined to be the flare start time. The flare end time was defined as the time at which the flux became smaller than  $1 + 3\sigma_2$  of the relative flux.

**Table 1:** Physical parameters of ZAMS stars in IC 2391 and IC 2602.

Object name	RA	Dec	$V$	$K$	Period	$\log N_R$	$\log R'_{\lambda 8542}$	Amp	Spot coverage	LC type
	[deg]	[deg]	[mag]	[mag]	[days]			[mag]		
(1)	(2)	(3)	(4)	(5)	(6)	(7)	(8)	(9)	(10)	(11)
IC 2391										
CI* IC2391 L32	130.57590	-53.90227	9.38	8.325	-	-0.31	-4.84	0.002	0.002	III
VXR PSPC 07	129.74920	-53.02395	9.63	8.272	-	0.04	-6.04	0.002	0.002	III
VXR PSPC 12	129.97104	-52.96579	11.86	9.793	3.69	-0.90	-4.34	0.030	0.039	I
VXR PSPC 22A	130.20459	-53.62927	11.08	9.272	2.31	-0.88	-4.34	0.025	0.030	I
VXR PSPC 44	130.55122	-53.10105	9.69	8.364	0.57	-0.36	-4.62	0.009	0.010	II
VXR PSPC 45A	130.56148	-52.93398	10.70	8.648	0.22	-2.12	-4.08	0.020	0.026	I
VXR PSPC 52	130.69420	-53.01704	10.34	8.991	2.15	-0.79	-4.70	0.013	0.016	I'
VXR PSPC 66	130.96793	-53.23327	9.73	8.594	0.92	-0.42	-4.98	0.004	0.005	I'
VXR PSPC 67A	130.98671	-52.68489	11.71	9.424	3.41	-0.93	-4.37	0.014	0.018	I
VXR PSPC 69A	130.99590	-53.56213	11.67	9.675	2.22	-1.12	-4.24	0.098	0.131	I
VXR PSPC 77A	131.41306	-52.43321	9.91	8.635	0.65	-1.11	-4.56	0.019	0.022	I
IC 2602										
CI* IC2602 W79	160.52952	-64.76884	11.57	-	6.55	-0.73	-4.57	0.011	0.014	III
RSP95 1	157.13011	-63.73767	11.57	9.537	3.85	-0.96	-4.33	0.026	0.033	I'
RSP95 7	157.93717	-63.48943	9.21	8.212	-	-0.11	-5.00	0.001	0.001	III
RSP95 10	158.11917	-65.10722	12.77	-	3.16	-1.18	-4.21	0.068	0.099	I'
RSP95 14	158.41530	-64.78116	11.57	9.572	2.73	-1.11	-4.25	0.020	0.025	I'
RSP95 29	159.15815	-64.79828	12.73	9.976	2.22	-1.34	-4.20	0.054	0.074	I
RSP95 35	159.57360	-64.13512	10.59	9.078	2.46	-0.71	-4.32	0.018	0.021	I'
RSP95 43	159.98321	-63.99169	12.14	9.622	0.78	-1.66	-3.92	0.103	0.141	I
RSP95 52	160.21399	-64.71329	12.19	9.555	0.39	-1.95	-4.12	0.145	0.206	I
RSP95 58	160.67298	-64.35120	10.52	8.840	0.57	-1.57	-4.18	0.038	0.046	I
RSP95 59	160.73377	-63.93087	11.86	9.537	1.31	-1.43	-4.16	0.066	0.089	I
RSP95 66	161.02838	-63.99307	11.07	9.311	3.28	-0.80	-4.46	0.028	0.035	I'
RSP95 68	161.05806	-64.77426	11.32	8.750	0.99	-1.55	-4.05	0.038	0.050	I'
RSP95 70	161.09396	-64.25837	10.92	9.322	4.25	-0.47	-4.59	0.018	0.021	I
RSP95 72	161.24842	-65.03863	10.89	9.157	1.05	-1.30	-4.15	0.048	0.060	I
RSP95 79	161.36767	-64.22918	9.08	7.989	0.75	-0.24	-4.73	0.003	0.003	I'
RSP95 80	161.37445	-64.42227	10.66	8.278	7.25	-0.69	-4.54	0.013	0.018	III
RSP95 83	161.56180	-64.04946	10.7	9.102	1.74	-1.08	-4.37	0.008	0.010	I'
RSP95 85	161.61995	-64.13266	9.87	8.680	1.33	-0.80	-4.91	0.003	0.004	I'
RSP95 89	161.71584	-63.57105	12.97	9.942	4.73	-1.01	-4.26	0.081	0.119	I
RSP95 92	162.07663	-64.16482	10.26	8.505	1.93	-0.82	-4.42	0.024	0.028	I
RSP95 95A	162.45167	-64.77457	11.73	9.480	1.22	-1.46	-4.20	0.007	0.009	I

References for parameters. (4)  $V$ -mag: Marsden et al. (2009). (5)  $K_s$ -mag: 2MASS survey (Cutri et al. 2003). (6) Period: Yamashita et al. (2022), <sup>a</sup>Patten & Simon (1996) and <sup>b</sup>Barnes et al. (1999). (7)(8)(9) The Rossby number  $N_R$ , the ratio of the surface flux of the Ca II IRT emission line at  $\lambda 8542$  to the stellar bolometric luminosity  $R'_{\lambda 8542}$ , and the amplitudes of the light curve: Yamashita et al. (2022).



### 3 Results

The rotational periods of the ZAMS stars in IC 2391 and IC 2602 range from 0.22 – 7.25 days. The amplitudes of the light curves range from 0.001 – 0.145 mag. The measured periods and amplitudes are similar to those of 88 ZAMS stars in Pleiades (Rebull et al. 2016a). Previous ground-based observation (Messina et al. 2011) also detected a variation of 0.2 mag in the brightness of 8 ZAMS stars in IC 2391 (namely, VXR PSPC 12, VXR PSPC 14, VXR PSPC 22A, VXR PSPC 35A, VXR PSPC 69, VXR PSPC 70, VXR PSPC 72, VXR PSPC 76A).

Figure 2 shows four examples of light curves. We categorized the light curves into the following groups:

- I) Single frequency: the star has a single period. A single spot or spot group is interpreted as rotating into and out of view.
- I') Possible shape changer: subcategory of type I) single frequency. The star usually has a single period. Shape of the light curve changes over the campaign, but not enough such that a separate period can be derived.
- II) Beater: the light curve appears to have a beating signature. The star has multi periods. Spot or spot group evolution and/or strong latitudinal differential rotation are suggested.
- III) Complex variability; the light curve has periodicity but seems complex. It is considered that the star has multiple sunspot groups.

Single frequency and beater are all classes found in Rebull et al. (2016b). For the 33 ZAMS stars in IC 2391 and IC 2602, we categorized 16 ZAMS stars as type I) single frequency, 11 ZAMS stars as type I') possible shape changer, 1 ZAMS star as type II) beater, and 5 ZAMS stars as type III) complex variability (table 2).

The apparent area of the spot,  $A_{\text{spot}}$ , was estimated from the amplitude of light variation ( $\Delta F/F$ ) using the following equation (Notsu et al. 2013; Shibata et al. 2013):

$$A_{\text{spot}} = \frac{\Delta F}{F} A_{\frac{1}{2}\text{star}} \left[ 1 - \left( \frac{T_{\text{spot}}}{T_{\text{eff}}} \right)^4 \right]^{-1}, \quad (1)$$

where  $A_{\frac{1}{2}\text{star}}$  is the effective area of the stellar hemisphere.  $T_{\text{spot}}$  and  $T_{\text{eff}}$  are the temperature of the starspot and photosphere of the star. We applied eq. (4) of Notsu et al. (2019). It is an empirical equation on the temperature difference between photosphere and spot,  $T_{\text{eff}} - T_{\text{spot}}$ , deduced from Berdyugina et al. (2005).

The starspot coverages,  $A_{\text{spot}}/A_{\frac{1}{2}\text{star}}$ , are estimated to be 0.1 – 21% for the ZAMS stars in IC 2391 and IC 2602. The mean coverage of each group is listed in table 2. ZAMS stars with single frequency have the largest mean spot area, and possible shape changer ZAMS stars have the second



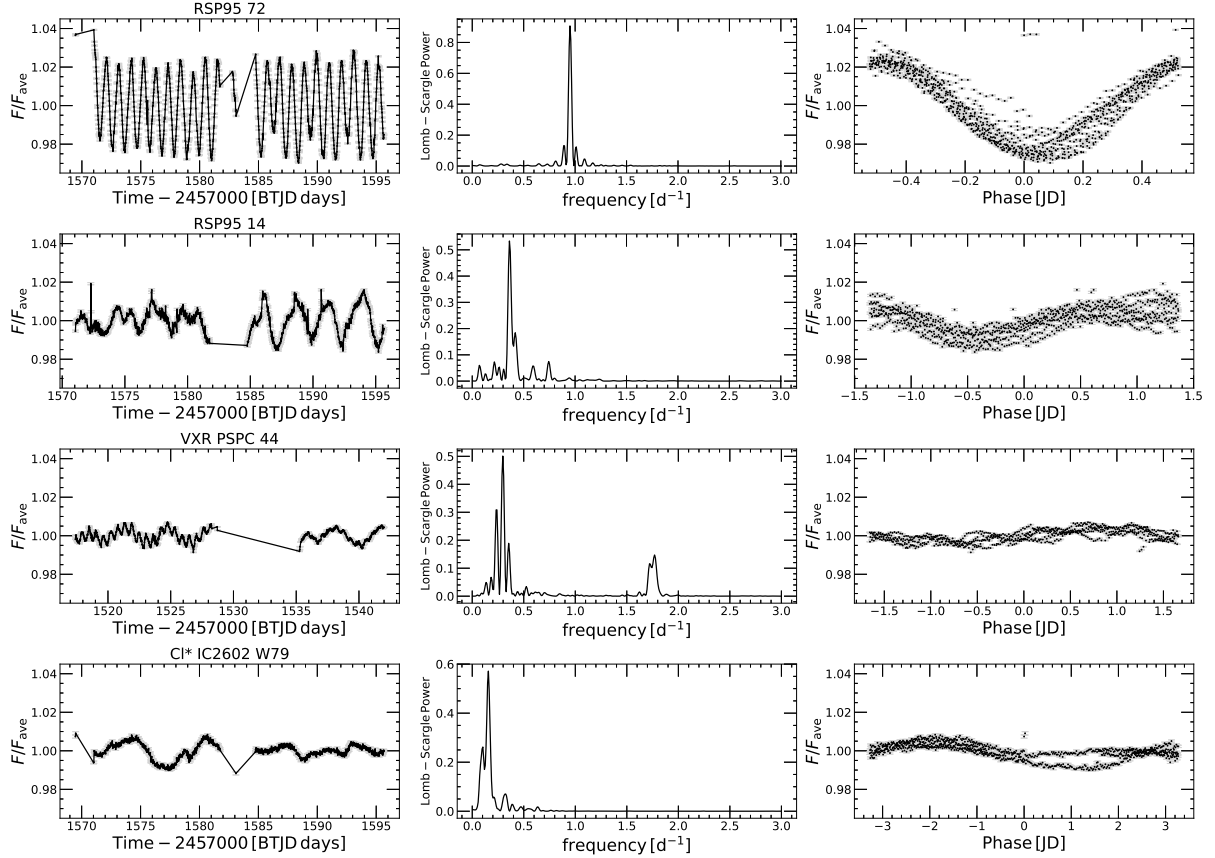


**Fig. 2:** Four examples of the light curves of ZAMS stars. The four features of the light curve, I) single frequency, I') possible shape changer, II) beater, and III) complex variability, are presented in order from the top to the bottom. Left column: full light curve; middle column: Lomb-Scargle periodogram; right column: phased light curve. Data points greater than  $3\sigma_1$  above the average flux were removed from the phased light curve.

largest values. The mean spot area of the beater and complex variability ZAMS stars are as same as the Solar value;  $\lesssim 1\%$ .

**Table 2:** Light curve groups and mean spot coverage of the 33 ZAMS stars

Features of the light curve	Number		Mean spot coverage [%]	
	IC 2391	IC 2602	IC 2391	IC 2602
I) Single frequency	6	10	$4.43 \pm 4.33$	$7.93 \pm 6.15$
I') Possible shape changer	2	9	$1.01 \pm 0.79$	$3.12 \pm 2.97$
II) Beater	1	0	1.00	-
III) Complex variability	2	3	$0.19 \pm 0.03$	$1.09 \pm 0.86$

The middle column of figure 2 shows examples of Lomb-Scargle periodograms. The FAP for the strongest peaks was calculated to be  $3 \times 10^{-290} - 0.007$ . *TESS* data was not obtained for several

days in the middle of the observation period. This leads to aliasing on the side of the strongest peak in the periodogram. When we split the light curve at the center time and applied Lomb–Scargle periodogram analysis, the aliasing disappeared.

**Table 3:** List of detected flares

Object name	$N_{\text{flare}}$	Flare rate	start	end	Duration time	$E_{\text{flare}}$
		[ $\text{d}^{-1}$ ]	–2457000[BTJDDays]		[s]	[erg]
(1)	(2)	(3)	(4)	(5)	(6)	(7)
IC 2309						
VXR PSPC 7	1	0.061	1527.732	1527.911	15500	$2.79 \times 10^{34}$
VXR PSPC 22A	2	0.119	1521.507	1521.691	15900	$1.10 \times 10^{34}$
			1538.712	1538.893	15600	$3.57 \times 10^{34}$
VXR PSPC 67A	1	0.066	1522.810	1523.031	19100	$4.99 \times 10^{33}$
IC 2602						
RSP95 14	4	0.211	1572.245	1572.394	12900	$9.19 \times 10^{33}$
			1589.550	1589.651	8700	$9.09 \times 10^{33}$
			1590.634	1590.788	13300	$4.49 \times 10^{33}$
			1594.010	1594.113	8900	$2.39 \times 10^{33}$
RSP95 43	1	0.049	1576.154	1576.233	6800	$1.09 \times 10^{33}$
RSP95 59	1	0.049	1595.024	1595.061	3200	$3.59 \times 10^{33}$
RSP95 66	1	0.049	1571.844	1571.953	9400	$6.49 \times 10^{33}$
RSP95 68	5	0.241	1578.423	1578.485	5400	$6.00 \times 10^{33}$
			1579.994	1580.064	6000	$9.59 \times 10^{33}$
			1580.417	1580.671	21900	$3.79 \times 10^{33}$
			1585.552	1585.652	8600	$1.55 \times 10^{34}$
			1586.795	1586.872	6700	$1.69 \times 10^{33}$
RSP95 72	1	0.050	1575.538	1575.639	8700	$1.66 \times 10^{34}$
RSP95 83	1	0.048	1586.471	1586.517	4000	$3.19 \times 10^{33}$
RSP95 89	1	0.050	1578.693	1579.124	37200	$1.32 \times 10^{34}$
RSP95 95A	2	0.096	1571.429	1571.710	24300	$2.10 \times 10^{34}$
			1588.191	1588.419	19700	$2.13 \times 10^{34}$

We also detected 21 flares in the light curves of 12 ZAMS stars in IC 2391 and IC 2602. The properties of each flare are listed in table 3. Their peak amplitude and duration time range from 0.3% to 5.2% and from 3200 s to 37200 s, respectively. For the case of the first flare shown in figure 1,

the relative flux and the duration are 2.0% and 2.4h, respectively. As we will discuss in section 4.4, the total bolometric energy of the flare is estimated to be  $\sim 10^{33} - 10^{35}$  erg. It is comparable of that of superflares detected in Maehara et al. (2012), in which the energy of the superflare is calculated to be 100 times larger than those of solar flares, i.e.  $10^{33}$  to  $10^{36}$  erg. The occurrence frequency of flares can be estimated from the number of observed flares, the number of observed stars, and the length of the observation period. In this study, 21 flares were detected from the 33 ZAMS stars in the observational period, so that the occurrence frequency of flares is calculated to be 10.9 flares per year per star. Maehara et al. (2012) detected 14 superflares from data collected from approximately 14,000 slowly rotating G-type main-sequence stars over 120d. The occurrence frequency of superflares was  $2.9 \times 10^{-3}$  flares per year per star. Therefore, superflares occur more frequently on ZAMS stars than on main-sequence stars.

## 4 Discussion

### 4.1 Stellar chromospheric activity and starspots of ZAMS stars

Notsu et al. (2015b) indicated that the Sun and superflare stars show a rough positive correlation between the amplitude of the light curve and the  $r_0(8542)$  index, the residual core flux normalized by the continuum level at the line core of the Ca II IRT. They claimed that the magnetic field strengths of superflare stars are higher than that of the Sun.

We investigated the relationship between the strength of the Ca II IRT emission line ( $\lambda 8542 \text{ \AA}$ ) and the amplitude of the light curve for the ZAMS stars in IC 2391, IC 2602, and the Pleiades cluster. We obtained the amplitude of the light curve of the ZAMS stars in the Pleiades cluster from Rebull et al. (2016a).  $R'_{\lambda 8542}$  for the ZAMS stars in IC 2391 and IC 2602 was already calculated in Paper I, as listed in table 1. We also obtained  $R'_{\lambda 8542}$  for the ZAMS stars in the Pleiades cluster from Stauffer et al. (1997). We also compare the relationship with the superflare stars studied in Notsu et al. (2015b). With  $F_{\lambda 8542}$  and  $T_{\text{eff}}$  listed in Notsu et al. (2015a, b), we calculated  $R'_{\lambda 8542}$  for the superflare stars (table 4) as

$$R'_{\lambda 8542} = \frac{F_{\lambda 8542}}{\sigma T_{\text{eff}}^4}, \quad (2)$$

where  $\sigma$  is Stefan-Boltzmann's constant.

Figure 3 shows that the ZAMS stars with a large light curve amplitude have large  $R'_{\lambda 8542}$ . The  $R'_{\lambda 8542}$  and light curve amplitudes of ZAMS stars are approximately two orders of magnitude larger than those of the Sun. We also found that the ZAMS stars are located on the extensions of the superflare stars (Notsu et al. 2015b). This result suggests that superflare stars link the properties of the Sun to those of the ZAMS stars of ages between 30 and 120 Myr. The ZAMS stars belonging in

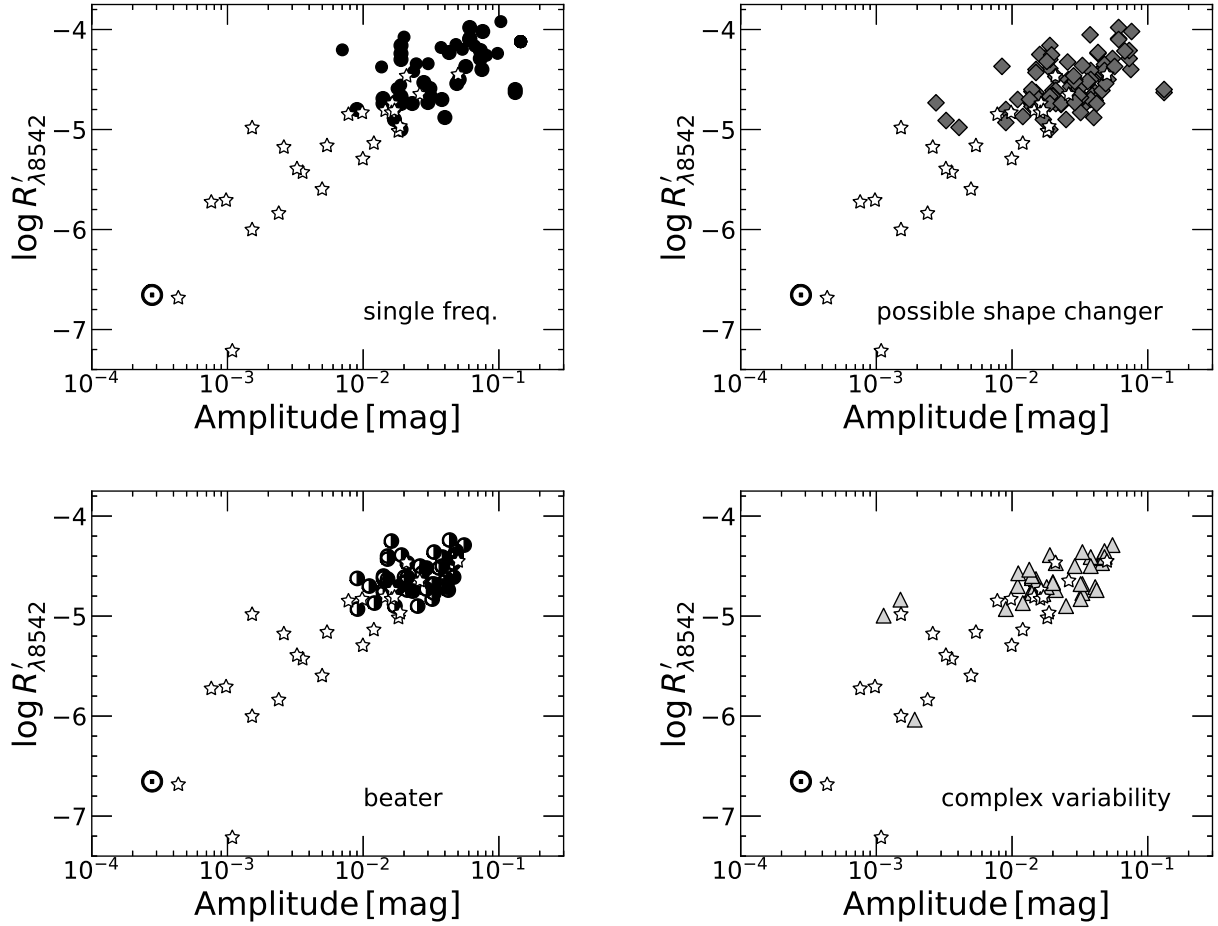


**Fig. 3:** Relationship between the amplitude of the light curve and the ratio of the surface flux of the Ca II IRT emission line ( $\lambda 8542 \text{ \AA}$ ) to the stellar bolometric luminosity,  $R'_{\lambda 8542}$  of the ZAMS stars in IC 2391, IC 2602, and the Pleiades cluster. The filled circles denote the ZAMS stars with single frequency. The gray diamonds represent the possible shape changer ZAMS stars. The half-filled circles denote the beater ZAMS stars. The light gray triangles show the ZAMS stars with complex variability. Star marks represent superflare stars (Notsu et al. 2015b). The light variations and  $R'_{\lambda 8542}$  of the ZAMS stars are as large as those of the most active superflare stars and two orders larger than those of the Sun. The ZAMS stars are located on the extensions of the superflare stars. This suggests that superflare stars link the properties of the Sun to those of the ZAMS stars of ages between 30 and 120 Myr.

each open cluster are almost evenly distributed. For the ZAMS stars in IC 2391, IC 2602, and the Pleiades cluster, the mean amplitudes are calculated to  $0.025 \pm 0.023$  mag,  $0.081 \pm 0.060$  mag, and  $0.036 \pm 0.030$  mag, respectively. Their mean  $R'_{\lambda 8542}$  are  $10^{-4.79 \pm 0.22}$ ,  $10^{-4.54 \pm 0.29}$ , and  $10^{-4.57 \pm 0.22}$ . The difference of their average values differ less than  $1\sigma$ .

Objects with different types of light curves seem to be unevenly distributed in figure 3, as represented by the colors of the symbols. The ZAMS stars with single frequency have larger light curve amplitudes and larger  $R'_{\lambda 8542}$  compared with other types, whereas the ZAMS stars with complex variability have smaller light curve amplitudes and smaller  $R'_{\lambda 8542}$  compared with other types. The possible shape changer ZAMS stars tend to be located between the ZAMS stars with single frequency and the ZAMS stars with complex variability. The relationship between the type of light curve and the magnetic activity will be discussed in the next sub-section.

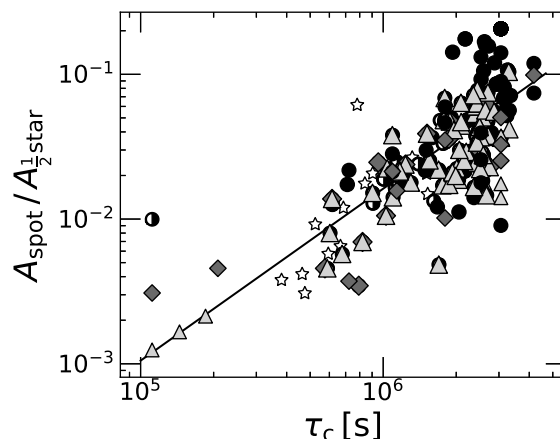


**Fig. 4:** Coverage of the starspot,  $A_{\text{spot}}/A_{\frac{1}{2}\text{star}}$ , as a function of the convection turnover time,  $\tau_c$  of the ZAMS stars in IC 2391, IC 2602, and the Pleiades cluster. The filled circles denote the ZAMS stars with single frequency. The gray diamonds show the possible shape changer ZAMS stars. The half-filled circle denotes the beater ZAMS star. The open triangles represent the ZAMS stars with complex variability. The star marks represent superflare stars (Notsu et al. 2015b). The solid line indicates the least squares linear fit line of all the objects shown here.  $A_{\text{spot}}/A_{\frac{1}{2}\text{star}}$  shows a positive correlation with  $\tau_c$ .

Figure 4 shows  $A_{\text{spot}}/A_{\frac{1}{2}\text{star}}$  as a function of the convective turnover time,  $\tau_c$  of the ZAMS stars in IC 2391, IC 2602, and the Pleiades cluster, and the superflare stars listed in Notsu et al. (2015b). In Paper I, we estimated the  $\tau_c$  values of the ZAMS stars using the  $\tau_c$  models for stars with the age of 50 Myr (IC 2391) and 30 Myr (IC 2602) presented in Landin (2010). We also estimated  $\tau_c$  for 130 Myr (the Pleiades) using the same method. For the ZAMS stars with  $T_{\text{eff}} > 6180\text{K}$ , we applied the approximation of  $\tau_c$  of Noyes et al. (1984). We also estimated  $\tau_c$  for the solar-type superflare stars (Notsu et al. 2015b) by applying the approximation of  $\tau_c$  of Noyes et al. (1984), where  $(B - V)_0$  is

referenced from Reinhold et al. (2015). We have estimated  $A_{\text{spot}}/A_{\frac{1}{2}\text{star}}$  with eq (1), as mentioned above.  $T_{\text{eff}}$  values of the Pleiades members and the solar-type superflare stars are taken from *Gaia* Data Release 2 (DR2; Gaia Collaboration 2018) and Notsu et al. (2015b), respectively.

Figure 4 indicated that  $A_{\text{spot}}/A_{\frac{1}{2}\text{star}}$  shows a positive correlation with  $\tau_c$ . The linear fit,  $A_{\text{spot}}/A_{\frac{1}{2}\text{star}} = 10^{-8.7} \cdot \tau_c^{1.2}$ , was derived.  $\tau_c$  used in this study is the local convective turnover time. According to the result of Jung & Kim (2007), there is an approximately linear relationship between  $\tau_c$  and the global convective turnover time,  $\tau_g$ . For a  $1 M_{\odot}$  star at ZAMS, we obtain  $\tau_g = 1.7\tau_c$ . Argiroffi et al. (2016) investigated the relationship between the ratio of the thickness of the convective zone to the stellar radius,  $H_c/R_*$  and  $\tau_g$ . We derived a linear fit as  $\tau_g [\text{d}] = 10^{3.1} \cdot (H_c/R_*)^{2.2}$ .

$$\begin{cases} A_{\text{spot}}/A_{\frac{1}{2}\text{star}} = 10^{-8.7} \cdot \tau_c^{1.2} \\ \tau_g = 1.7\tau_c \\ \tau_g [\text{d}] = 10^{3.1} \cdot (H_c/R_*)^{2.2} \end{cases} \quad (3)$$

Therefore

$$\frac{A_{\text{spot}}}{A_{\frac{1}{2}\text{star}}} = 4.6 \left( \frac{H_c}{R_*} \right)^{2.6}. \quad (4)$$

When we assume that the geometry of a starspot is single circle whose diameter is  $D_{\text{spot}}$ , we can obtain

$$\left( \frac{D_{\text{spot}}}{2R_*} \right)^2 = 4.6 \left( \frac{H_c}{R_*} \right)^{2.6}. \quad (5)$$

Therefore,

$$D_{\text{spot}} = 2\sqrt{4.6H_c^{2.6}} \sim 4.3H_c^{1.3}. \quad (6)$$

Numerical simulation indicates that for a large sunspot, the ratio of the horizontal size at the photosphere to  $H_c$  ranges from 2.04 to 6.75 (Vickers 1971). Mullan (1973) discussed the relationship between the thickness of the convection zone and the size of a starspot. They considered that the depth of the spot,  $H_s$ , is equal to the depth of the convection zone,  $H_c$ , which yields  $2.04 < D_{\text{spot}}/H_c < 6.75$ . We derived  $D_{\text{spot}}/H_c \sim 4.3$ , which is well within the values presented in Mullan (1973).

## 4.2 Starspots and Rotation-Activity Relationship

In this section, we examine the relationship between the spot area and the rotation-activity relationship. In Paper I, we calculated  $N_R$  for the ZAMS stars in IC 2391 and IC 2602. We also calculated  $N_R$  for the Pleiades members and the superflare stars listed in Notsu et al. (2015b). Their  $P$  values were taken from Rebull et al. (2016b) and Notsu et al. (2015b), respectively.  $N_R$  for the superflare stars is shown in table 4. The relationship between  $N_R$  and the ratio of the surface flux of the Ca II

**Table 4:** Rossby numbers and  $R'$  of solar-type superflare stars listed in Notsu et al. (2015b)

Object name	$\log N_{\text{R}}$	$\log R'_{\lambda 8542}$
(1)	(2)	(3)
KIC 4742436	-0.48	-5.60
KIC 6865484	0.23	-4.85
KIC 7354508	0.34	-5.16
KIC 7420545	0.31	-5.14
KIC 8802340	-0.13	-5.02
KIC 9583493	-0.25	-4.81
KIC 9652680	-0.78	-4.45
KIC 10471412	0.44	-5.18
KIC 10528093	-0.10	-4.47
KIC 11140181	0.00	-4.74
KIC 11303472	-0.11	-4.83
KIC 11390058	0.35	-5.43
KIC 11455711	0.24	-5.29
KIC 11494048	0.53	-5.39
KIC 11764567	0.22	-4.97
KIC 12266582	-0.18	-4.81

IRT emission line to the stellar bolometric luminosity,  $R'_{\lambda 8542}$ , is shown in figure 5. For the ZAMS stars in IC 2391, IC 2602, and the Pleiades cluster with  $N_{\text{R}} > 10^{-1.1}$ ,  $R'_{\lambda 8542}$  increases with decreasing  $N_{\text{R}}$  until it saturates. For the ZAMS stars with  $N_{\text{R}} < 10^{-1.1}$ ,  $R'_{\lambda 8542}$  reaches a constant level. All the superflare stars and the Sun belong to the unsaturated regime. The ZAMS stars belonging in each open cluster are almost evenly distributed.

Objects with a smaller  $N_{\text{R}}$  have both a saturated  $R'_{\lambda 8542}$  and a larger light curve amplitude (figure 5). It is known that small  $N_{\text{R}}$  objects are strongly activated by their dynamo process. The dynamo process is considered to induce a strong magnetic field, resulting in large starspots and saturated strong emission lines. The Ca II saturation is consistent with the existence of a large-scale starspot or starspot group.

Figure 6 shows the relationship between  $R'_{\lambda 8542}$  and  $N_{\text{R}}$  of the ZAMS stars in IC 2391, IC 2602, and the Pleiades cluster. We noticed that the ZAMS stars with single frequency or possible shape change have small  $N_{\text{R}}$  and large  $R'_{\lambda 8542}$ . By combining with figure 5, it is suggested that those objects show larger light curve amplitude, indicating huge spot/spot groups. The ZAMS stars with



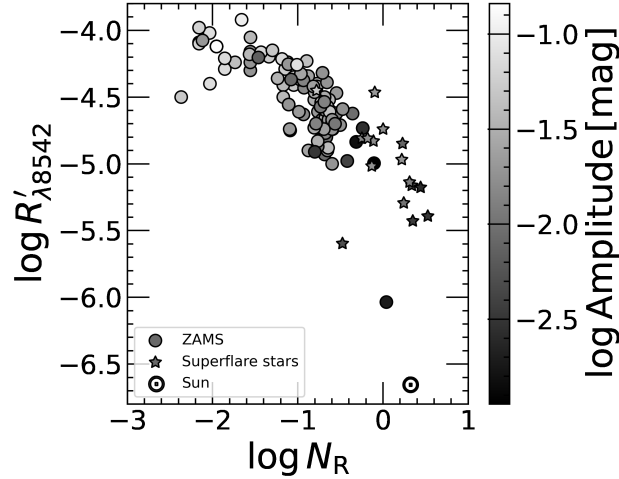


**Fig. 5:** Relationship between the ratio of the surface flux of the Ca II emission line ( $\lambda 8542 \text{ \AA}$ ) to the stellar bolometric luminosity,  $R'_{\lambda 8542}$ , and the Rossby number,  $N_R$ , of the ZAMS stars in IC 2391, IC 2602, and the Pleiades cluster (circles). Star marks represent superflare stars (Notsu et al. 2015b). The gray scale of all the symbols represents the amplitude of the light curve. Objects with a smaller  $N_R$  have both a saturated  $R'_{\lambda 8542}$  and a larger light curve amplitude.

beat or complex variability have large  $N_R$ , small  $R'_{\lambda 8542}$ , and smaller light curve amplitude. This result suggests that those ZAMS stars do not have huge spot/spot groups.

We consider that the strong magnetic field generates a limited number of large starspots. With *Kepler* observations, Reinhold et al. (2020) revealed that 369 stars with near-solar rotational periods have much stronger and more regular light variation than the Sun. Isik et al. (2020) constructed the light curve model of such stars by injecting active regions on stellar surfaces with highly inhomogeneous distribution compared with the Sun. The injected active region consists of spot groups and faculae. They used wavelength-dependent contrast models of faculae and spots on the Sun calculated by Unruh, Solanki, & Fligge (1999). Different activity levels lead to different types of light curves, i.e., periodic, strong variation, and complex variation. They qualified the activity level in terms of the chromospheric S-index. By extrapolating the relationship between the disk coverage by spots and the S-index of the Sun (Shapiro et al. 2014), they obtained the S-index for a more active star with a given light curve. Isik et al. (2020) found that the light curve amplitude increases with larger S-index because of the increasing occurrence of active regions. Active longitude nesting, in which active regions appear on the opposite side, leads to highly regular variability. The regularity and light curve amplitude decrease for small S-index objects. As mentioned above,  $R'_{\lambda 8542}$  of the ZAMS stars in IC 2391, IC 2602, and the Pleiades cluster with single frequency tend to be saturated, and that of the ZAMS stars with complex variability is relatively small. This result supports the assumption in

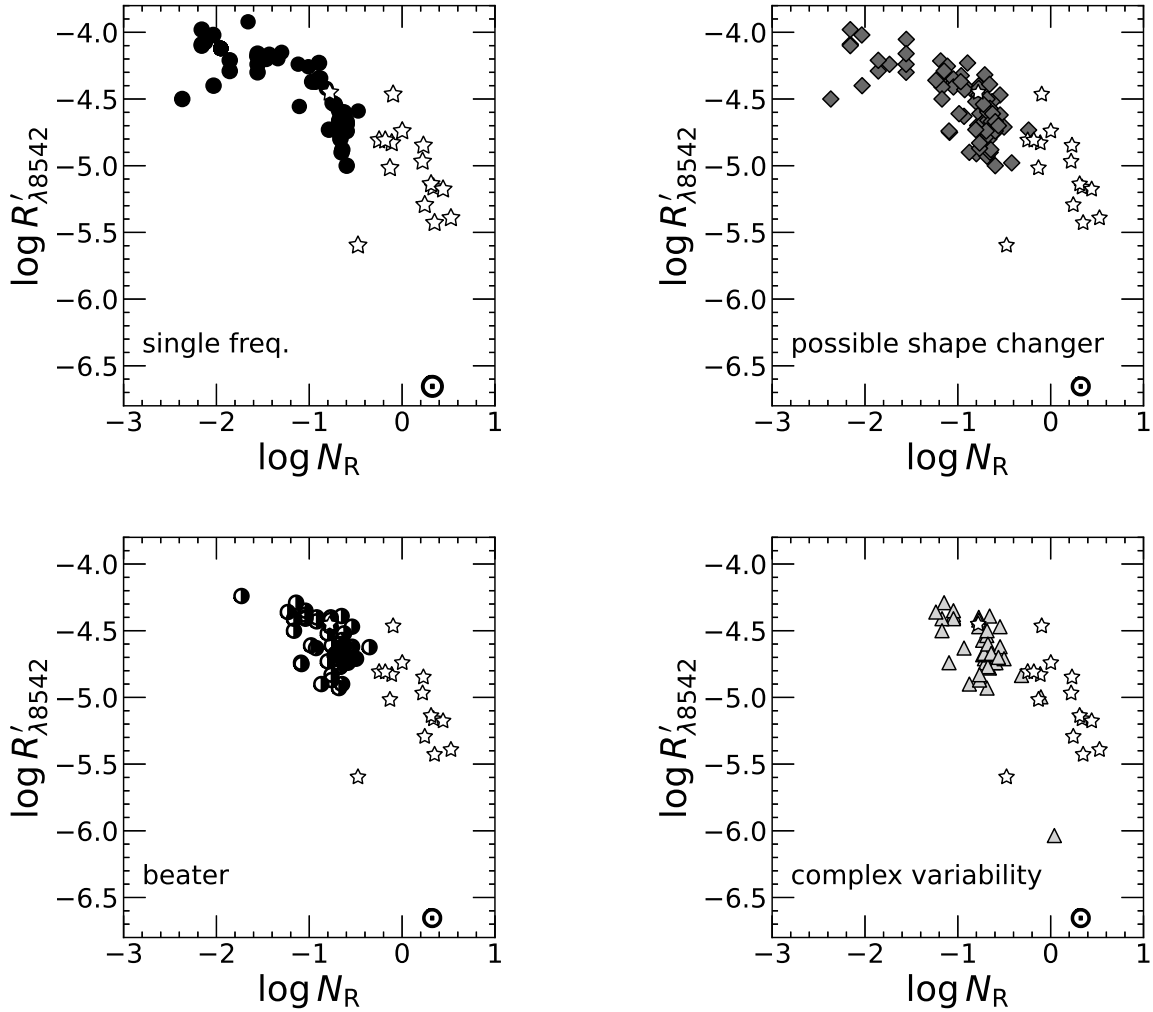


**Fig. 6:** Relationship between the ratio of the surface flux of the Ca II emission line ( $\lambda 8542 \text{ \AA}$ ) to the stellar bolometric luminosity,  $R'_{\lambda 8542}$ , and the Rossby number,  $N_R$ , of the ZAMS stars in IC 2391, IC 2602, and the Pleiades cluster. The filled circles denote ZAMS stars with single frequency. The gray diamonds denote the possible shape changer ZAMS stars. The half-filled circles denote the beater ZAMS stars. The open triangles denote ZAMS stars with complex variability. Star marks represent superflare stars (Notsu et al. 2015b). The ZAMS stars with single frequency or possible shape change have small  $N_R$ , large  $R'_{\lambda 8542}$ , and larger light curve amplitude, while the ZAMS stars with beat or complex variability have large  $N_R$ , small  $R'_{\lambda 8542}$ , and smaller light curve amplitude.

Isik et al. (2020) that the active regions are inhomogeneously distributed on the surface of an active star.

### 4.3 Period-Color Distribution

Rebull et al. (2020) investigated the relationship between  $(V - K_s)_0$  and  $P$  with  $K2$  data for six clusters: Rho Oph, Taurus, Upper Sco, Taurus foreground, Pleiades, and Prasepe (1 – 790 Myr) and discussed spin-down evolution to the main-sequence.

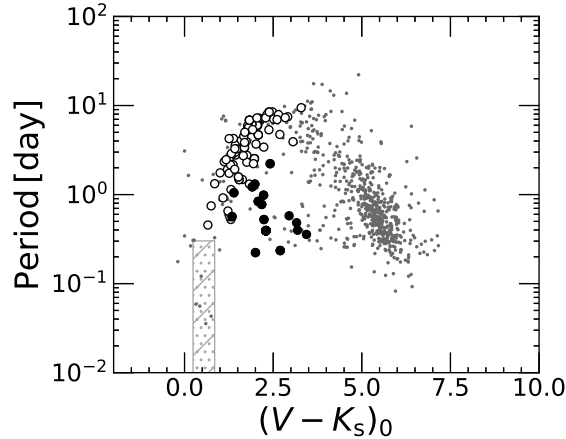


**Fig. 7:** Relationship between the  $(V - K_s)_0$  color and the rotational period of ZAMS stars in IC 2391, IC 2602, and the Pleiades cluster. The filled circles show the ZAMS stars whose Ca II IRT emission lines are saturated ( $R'_{\lambda 8542} \sim 10^{-4.2}$ ). The open circles show the ZAMS stars with  $R'_{\lambda 8542} < 10^{-4.2}$  whose Ca II IRT emission lines are unsaturated. The tiny circles denote the Pleiades members examined by Rebull et al. (2016a) but whose Ca II IRT emission lines had not been observed in Stauffer et al. (1997). The hatched area represents  $0.24 < (V - K_s)_0 < 0.85$  and  $P \leq 0.3$  days. The ZAMS stars whose Ca II emission lines are saturated tend to be distributed in the lower part of the figure, while the ZAMS stars whose Ca II emission lines are unsaturated are located close to the majority of the Pleiades members.

We investigated the  $P$  of the members of IC 2391 and IC 2602 as a function of  $(V - K_s)_0$  (figure 7 and figure 8). We took the  $V$  magnitudes from Marsden et al. (2009) and the  $K_s$  magnitudes from the 2MASS survey (Cutri et al. 2003). These values are listed in table 1. The  $(V - K_s)$  values were converted to unreddened values,  $(V - K_s)_0$ , using the reddening parameters for the clusters;  $E(B - V) = 0.006$  for IC 2391 from Patten & Simon (1996) and  $E(B - V) = 0.04$  for IC 2602 from Braes (1961) were converted to  $E(V - K_s) = 0.016$  and  $E(V - K_s) = 0.110$  for IC 2391 and IC 2602 by multiplying the  $E(V - K_s)/E(B - V)$  value given in Rieke & Lebofsky (1985).

We found that the ZAMS stars in IC 2391, IC 2602, and the Pleiades cluster whose Ca II emission lines are saturated tend to be distributed in the lower part of the figure 7, while the ZAMS stars whose Ca II emission lines are unsaturated are located close to the majority of the Pleiades

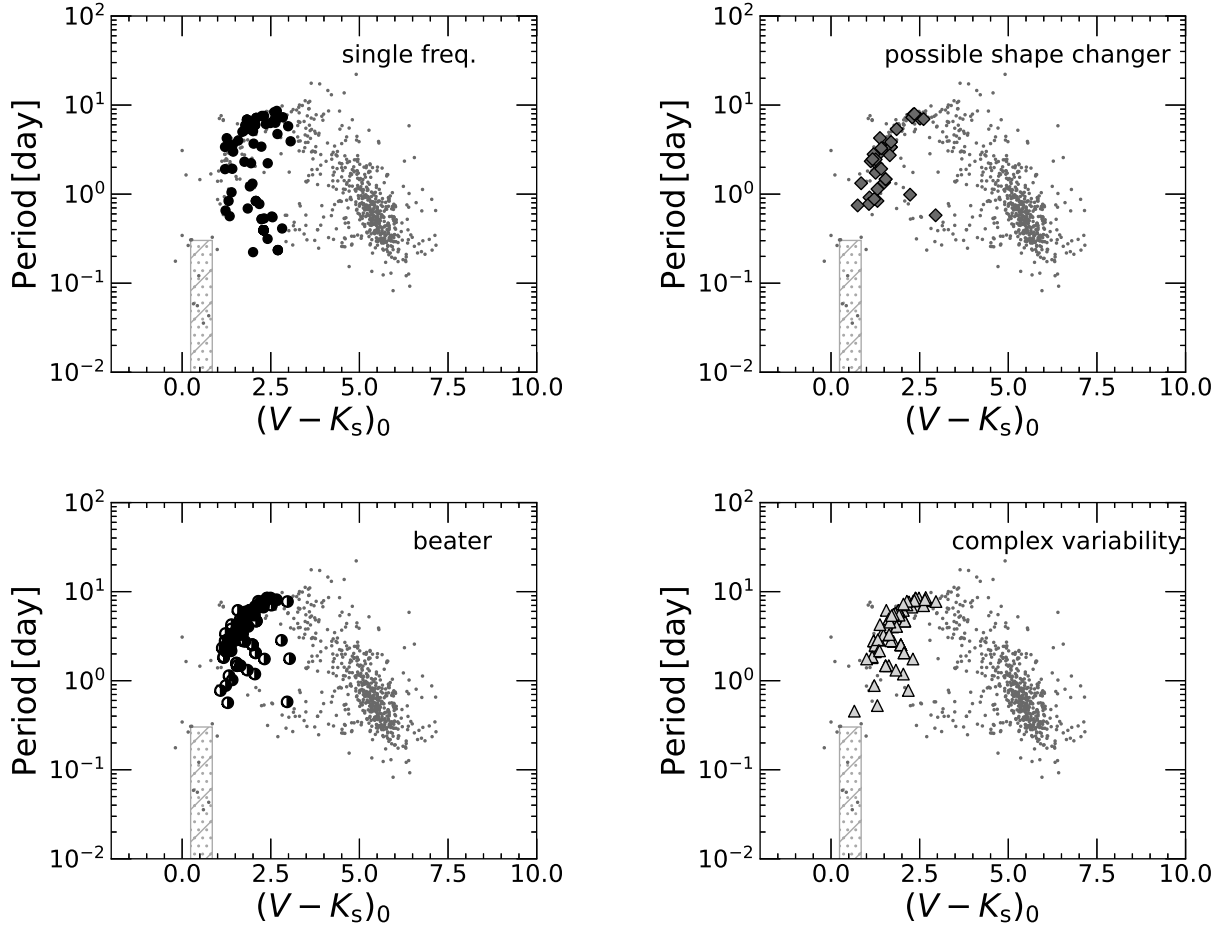


**Fig. 8:** Relationship between the  $(V - K_s)_0$  color and the rotational period of ZAMS stars in IC 2391, IC 2602, and the Pleiades cluster. The filled circles denote the ZAMS stars with single frequency. The gray diamonds denote the possible shape changer ZAMS stars. The half-filled circles denote the beater ZAMS stars. The open triangles denote the ZAMS stars with complex variability. The tiny circles denote the Pleiades members examined by Rebull et al. (2016a) but whose Ca II IRT emission lines had not been observed in Stauffer et al. (1997). The hatched area represents  $0.24 < (V - K_s)_0 < 0.85$  and  $P \leq 0.3$  days. Most of the ZAMS stars rotating rapidly have light curve with a single frequency period.

members. It is possible that the ZAMS stars whose Ca II emission lines are saturated have not reached the spin down stage yet. In figure 8, we also found that most of the ZAMS stars rotating rapidly have a single frequency period. These results obtained from figures 7 and 8 show that the ZAMS stars not reached the spin down stage have saturated Ca II emission lines and single frequency periods. As mentioned in the discussion on figure 6, the ZAMS stars with single frequency tend to have strong Ca II IRT emission lines. These results are consistent with Rebull et al. (2016b) and Stauffer et al. (2016), in which approximately half of the ZAMS stars rotating rapidly have sinusoidal light curves. Here, we do not think that stellar pulsation is the cause of the light variation. Rebull et al. (2016a) considered that only 1% of the Pleiades members are pulsators, including the  $\delta$  Sct-type, which have very small light curve amplitudes,  $0.24 < (V - K_s)_0 < 0.85$ , and short rotational periods. No ZAMS stars in IC 2391 and IC 2602 have both a short period and an early spectral type.

#### 4.4 Superflare

After removing the rotational light variations in the *TESS* light curves, we detected 21 flares from 12 ZAMS stars in IC 2391 and IC 2602. These flares show characteristics similar to those of solar-type main-sequence stars. figure 9 shows the relationship between the light curve amplitude and the number of the flares on the ZAMS stars in IC 2391 and IC 2602. More frequent flares are observed on the ZAMS stars with larger light curve amplitudes. We found no correlation between the rotational phase and the number of flares, which is also claimed in a study on M dwarfs (Doyle et al. 2018).

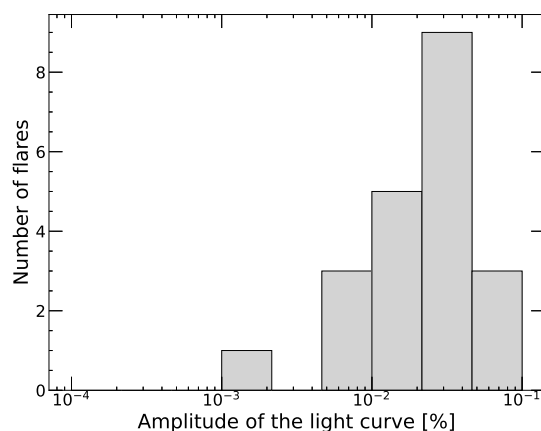


**Fig. 9:** Relationship between the light curve amplitude and the number of flares on the ZAMS stars in IC 2391 and IC 2602. More frequent flares are observed on the ZAMS stars with larger light curve amplitudes.

The energy of a flare can be estimated from the amplitude of a flare ( $\Delta F_{\text{flare}}/F$ ) and the duration time. A detailed description is presented in Shibayama et al. (2013) and their related studies.  $\Delta F_{\text{flare}}/F$  can be written as

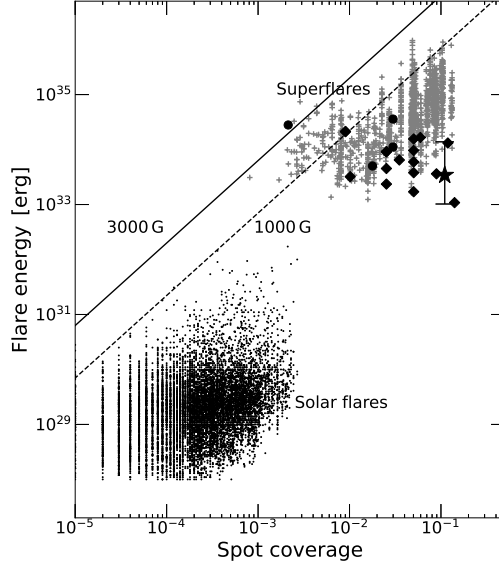


**Fig. 10:** Relationship between spot coverage,  $A_{\text{spot}}/A_{\frac{1}{2}\text{star}}$ , and flare energy,  $E_{\text{flare}}$ . Circles and diamonds denote flares on the ZAMS stars in IC 2391 and IC 2602, respectively. The star symbol represents the flare distribution of EK Dra detected by *TESS* (Namekata et al. 2022). The tiny circles show solar flares (Shibayama et al. 2013), and the cross symbols show superflares on Sun-like stars with  $T_{\text{eff}} = 5100 - 5600$  K. The black solid and dashed lines correspond to the analytical relationship between  $E_{\text{flare}}$  and  $A_{\text{spot}}$  for  $B = 3000$  G and  $1000$  G, respectively. For the flares on the ZAMS stars in IC 2391 and IC 2602, the energy is estimated to be  $\sim 10^{33} - 10^{35}$  erg, which is comparable with the energy of a superflare.

$$\frac{\Delta F_{\text{flare}}}{F} = \frac{A_{\text{flare}}}{A_{\frac{1}{2}\text{star}}} \frac{\int B(T_{\text{flare}}, \lambda) S(\lambda) d\lambda}{\int B(T_{\text{eff}}, \lambda) S(\lambda) d\lambda}, \quad (7)$$

where  $A_{\text{flare}}/A_{\frac{1}{2}\text{star}}$  is the fraction of the flare-emitting area normalized by the effective area of the stellar hemisphere. With the Stefan-Boltzman law regarding the photospheric luminosity and  $T_{\text{eff}}$  of the ZAMS stars in *Gaia* DR2, we estimated the stellar radius and converted it to  $A_{\frac{1}{2}\text{star}}$ .  $T_{\text{flare}}$  is the effective temperature of a flare component. We assumed that the spectral energy distribution of the flare component is similar to blackbody radiation, with an effective temperature of 10000 K (e.g., Hawley & Pettersen 1991; Hawley & Fisher 1992).  $B(T_{\text{flare}}, \lambda)$  is the Planck function, and  $S(\lambda)$  is the spectral response function of the *TESS* detector ( $\lambda 6000 - 10000$  Å; Ricker et al. 2015). We estimated  $A_{\text{flare}}$  with eq (7) and substituted it into eq (8), after which we obtained the bolometric luminosity of the flare,  $L_{\text{flare}}$ .

$$L_{\text{flare}} = \sigma T_{\text{flare}}^4 A_{\text{flare}}. \quad (8)$$

The total bolometric energy of a superflare,  $E_{\text{flare}}$ , is an integral of  $L_{\text{flare}}$  over the flare duration,

$$E_{\text{flare}} = \int L_{\text{flare}}(t) dt. \quad (9)$$

Figure 10 is a scatter plot of the flare energy,  $E_{\text{flare}}$ , as a function of spot coverage,  $A_{\text{spot}}/A_{\frac{1}{2}\text{star}}$ . In the figure, solar flares and superflares, including those of EK Draconis (EK Dra), are also shown. EK Dra is known as an active G-type ZAMS star that exhibits frequent flares. For EK Dra, we referenced the spot coverage from Strassmeier & Rice (1998), and the flare energy from Namekata et al. (2022). We found that the spot coverage of the ZAMS stars in IC 2391 and IC 2602 is similar to that of superflare stars. The energy of the flares is estimated to be  $\sim 10^{33} - 10^{35}$  erg, which is comparable with the energy of a superflare. One flare is above the analytical relationship for  $B = 3000$  G.

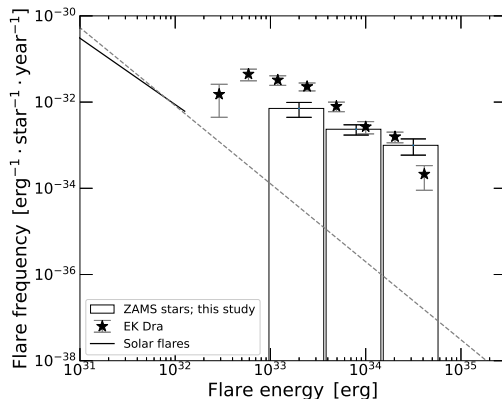


**Fig. 11:** Occurrence rate of flares on ZAMS stars and of solar flares. The histogram shows the frequency distribution of flares on the 12 ZAMS stars in IC 2391 and IC 2602 on which flares were detected. The star symbols represent the flare distribution of EK Dra detected by *TESS* (Namekata et al. 2022). The solid line indicates the power-law distribution of solar flares observed in hard X-rays (Crosby et al. 1993), with the distribution  $dN/dE \propto E^{-\alpha}$  with index  $\alpha \sim 1.8$ . The dashed line corresponds to the power-law distribution estimated from superflares in Sun-like stars and solar flares (Shibayama et al. 2013). The flare frequency on the 12 ZAMS stars is similar to that of EK Dra.

We compare the occurrence rate of flares on ZAMS stars in IC 2391 and IC 2602 with those of solar flares (figure 11). Flares with larger energy have a lower occurrence rate, the same as solar flares. For the 12 ZAMS stars from which flares were detected, we obtained the distribution  $dN/dE \propto E^{-\alpha}$  with index  $\alpha \sim 0.7$ . We found that the flare frequency on EK Dra is similar to that of our ZAMS stars.

Figure 12 shows the relationship between the flares and the rotation-activity. Most of the ZAMS stars in IC 2391 and IC 2602 on which the flares are detected are located in the saturated regime. Flares occur more frequently on the ZAMS stars having small  $N_R$ . Davenport (2016) show that GKM stars with small  $N_R$  show luminous flares. Medina et al. (2020) examined the relationship between  $N_R$  and the flare rate for mid- to late-M dwarfs. They found a high flare rate for small  $N_R$  stars. Our results indicate that small  $N_R$  objects experience superflares, even for ZAMS stars.



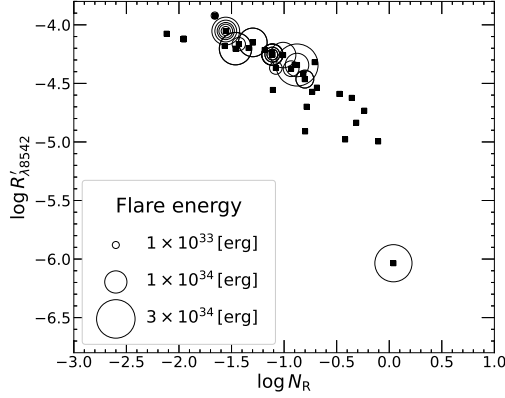


**Fig. 12:** The 21 flares are shown for the relationship between the ratio of the surface flux of the Ca II emission line ( $\lambda 8542 \text{ \AA}$ ) to the stellar bolometric luminosity,  $R'_{\lambda 8542}$ , and the Rossby number,  $N_R$ , of the ZAMS stars in IC 2391 and IC 2602 (squares). The flares and their energies are represented by open circles and their size, respectively. Most of the ZAMS stars on which the flares are detected are located in the saturated regime. Flares occur more frequently on the ZAMS stars having small  $N_R$ .

## 5 Conclusion

We analyzed the *TESS* light curves for the 33 ZAMS stars belonging to IC 2391 and IC 2602. Light variation was detected in all the ZAMS stars. This was considered to be caused by starspots. The amplitudes of the light curves range from 0.001 – 0.145 mag. The starspot coverages range from 0.1 – 21%.

1. The  $R'_{\lambda 8542}$  and of light curve amplitudes of ZAMS stars in IC 2391, IC 2602, and the Pleiades cluster are approximately two orders of magnitude larger than those of the Sun. These ZAMS stars are located on the extensions of the superflare stars and the Sun. This result suggests that superflare stars link the properties of the Sun to those of the ZAMS stars of ages between 30 and 120 Myr.
2. The ZAMS stars in IC 2391, IC 2602, and the Pleiades cluster with small  $N_R$  show a light curve with a single frequency or possible shape change. The light curves have large amplitude, indicating inhomogeneous longitudinal distribution of large starspots. They also show saturated chromospheric Ca II emission lines, and have not reached the spin-down period. Most of the flare events were detected on such objects in IC 2391 and IC 2602. Those energies are more than  $10^{33}$  erg, so that these flare events correspond to superflares.
3. The ZAMS stars in IC 2391, IC 2602, and the Pleiades cluster with large  $N_R$  show beat or a complex light curve with a small amplitude. They have weak Ca II emission lines. The superflare events are rare on such objects in IC 2391 and IC 2602.

# Acknowledgments

We wish to thank Dr. Notsu Y. and Dr. Namekata K. for comments. This paper includes data collected with the TESS mission, obtained from the MAST data archive at the Space Telescope Science Institute (STScI). M. Yamashita was supported by a scholarship from the Japan Association of University Women and would like to acknowledge them. This research was supported by a grant from the Hayakawa Satio Fund awarded by the Astronomical Society of Japan. Y. I. is supported by JSPS KAKENHI grant number 17K05390.

# References

- Allain, S., Fernandez, M., Martin, E. L., & Bouvier, J. 1996, *A&A*, 314, 173
- Argiroffi, C., Caramazza, M., Micela, G., et al. 2016, *A&A*, 589, A113
- Baliunas, S., Sokoloff, D., & Soon, W. 1996, *ApJ.*, 457, L99
- Barnes, S. A., Sofia, S., Prosser, C. F., & Stauffer, J. R. 1999, *ApJ*, 516, 263
- Barrado y Navascues, D., Stauffer, J. R., & Jayawardhana, R. 2004, *ApJ*, 614, 386
- Berdyugina, S. V. 2005, *LRSP*, 2, 8
- Braes, L. L. E. 1961, *MNRAS*, 20, 7B
- Crosby, N. B., Aschwanden, M. J., & Dennis, B. R. 1993, *SoPh*, 143, 275C
- Cutri, R. M., Skrutskie, M. F., van Dyk, S., et al. 2003, *VizieR Online Data Catalog: II/246*
- Davenport, J. R. A. 2016, *ApJ*, 829, 23
- D’Orazi, V., & Randich, S. 2009, *A&A*, 501, 553
- Doyle, L., Ramsay, G., Doyle, J. G., Wu, K., & Scullion, E. 2018, *MNRAS*, 480, 2153
- Feinstein, A. D., Montet, B. T., Foreman-Mackey, D., et al. 2019, *PASP*, 131
- Folsom, C. P., Petit, P., Bouvier, J., et al. 2016, *MNRAS*, 457, 580
- Fritzewski, D. J., Barnes, S. A., James, D. J., Järvinen, S. P., & Strassmeier, K. G. 2021, *A&A*, 656
- Gaia Collaboration, 2018, *A&A*, 616, A1
- Gallet, F., & Bouvier, J. 2015, *A&A*, 577, 1
- Haro, G., Chavira, E., & Gonzalez, G. 1982, *Boletín del Instituto de Tonantzintla*, 3, 3
- Ilin, E., Schmidt, S. J., Poppenhager, K., et al. 2021, *A&A*, 645, A42
- Isik, E., Shapiro, A. I., Solanki, S. K., & Krivova, N. A. 2020, *ApJL*, 901, L12
- Jung, Y. K., & Kim, Y.-C. 2007, *J. Astron. Space Sci.*, 24, 1
- Koch, D. G., Borucki, W. J., Basri, G., et al. 2010, *ApJL*, 713, 79
- Landin, N. R., Mendes, L. T. S., & Vaz, L. P. R. 2010, *A&A*, 510, 1
- Lanza, A. F., Rodonò, M., Pagano, I., Barge, P., & Llebaria, A. 2003, *A&A*, 403, 1135
- Maehara, H., Shibayama, T., Notsu, S., et al. 2012, *Nature*, 485, 478
- Marsden, S. C., Carter, B. D., & Donati, J.-F. 2009, *MNRAS*, 399, 888
- Medina, A. A., Winters, J. G., Irwin, J. M., & Charbonneau, D. 2020, *ApJ*, 905, 107
- Messina, S., Desidera, S., Lanzafame, A. C., Turatto, M., & Guinan, E. F. 2011, *A&A*, 532, A10
- Mullan, D. J. 1973, *ApJ*, 186, 105

Namekata, K., Maehara, H., Honda, S., et al. 2022, ApJL, 926, L5

Notsu, Y., Shibayama, T., Maehara, H., et al. 2013, ApJ, 771

Notsu, Y., Honda, S., Maehara, H., et al. 2015a, PASJ, 67, 32

Notsu, Y., Honda, S., Maehara, H., et al. 2015b, PASJ, 67, 33

Notsu, Y., Maehara, H., Honda, S., et al. 2019, ApJ, 876, 58

Noyes, R. W., Hamann, F. W., Baliunas, S. L., & Vaughan, A. H. 1984, AJ, 279, 763

Patten, B. M., & Simon, T. 1996, ApJS, 106, 489

Randich, S., Pallavicini, R., Meola, G., Stauffer, J. R., & Balachandran, S. 2001, A&A, 372, 862

Rebull, L. M., Stauffer, J. R., Bouvier, J., et al. 2016a, AJ, 152, 113

Rebull, L. M., Stauffer, J. R., Bouvier, J., et al. 2016b, AJ, 152, 114

Rebull, L. M., Stauffer, J. R., Cody, A. M., et al. 2020, AJ, 159, 273

Reinhold, T., & Gizon, L. 2015, A&A, 583, 65

Reinhold, T., Shapiro, A. I. A. I., Solanki, S. K. S. K., et al. 2020, Science, 368, 518

Ricker, G. R., Winn, J. N., Vanderspek, R., et al. 2014, J. Astron. Telescopes Instrum. Syst., 1, 014003

Rieke, G. H., & Lebofky, M. J. 1985, ApJ, 288, 618

Saar SH, Bookbinder JA. 1998, Cool Stars, Stellar Systems, and the Sun, 154, 1560

Scargle, J. D. 1982, AJ, 263, 835

Shapiro, A. I., Solanki, S. K., Krivova, N. A., et al. 2014, A&A, 569, 38

Shibayama, T., Maehara, H., Notsu, S., et al. 2013, ApJS, 209, 5

Stauffer, J. R., Hartmann, L. W., Prosser, C. F., et al. 1997, ApJ, 479, 776

Stauffer, J., Rebull, L., Bouvier, J., et al. 2016, AJ, 152, 115

Strassmeier, K. G., Rice, J. B., 1998, A&A, 330, 685

Unruh, Y. C., Solanki, S. K., & Fligge, M. 1999, A&A, 345, 635

Vickers, G. T. 1971, ApJ, 163, 363

Yamashita, M., Itoh, Y., & Takagi, Y. 2020, PASJ, 72, 80

Yamashita, M., & Itoh, Y. 2022, PASJ, accepted (Paper I)